Phase selection in the rare earth silicides

C. Eames, M. Reakes, and S. P. Tear*
Department of Physics, University of York, York YO10 5DD, United Kingdom

T. C. Q. Noakes and P. Bailey
STFC Daresbury Laboratory, Daresbury, Warrington WA4 4AD, United Kingdom

(Received 28 June 2010; revised manuscript received 28 August 2010; published 15 November 2010)

The rare earth silicides form islands with a tetragonal or a hexagonal structure that coexist when grown on the Si(100) surface. We show using medium energy ion scattering that it is possible to selectively grow one of these as a pure phase by controlling the mobility of the rare earth atoms as they are deposited. When dysprosium, holmium, and erbium are deposited onto a liquid nitrogen cooled substrate the hexagonal structural phase is formed after annealing. When erbium and holmium are deposited onto a hot substrate only the tetragonal phase results. For dysprosium silicide growth under conditions of high mobility causes approximately equal numbers of hexagonal and tetragonal islands to form. The system offers a means to obtain fine control over physical properties such as the Schottky barrier height.

DOI: 10.1103/PhysRevB.82.174112 PACS number(s): 68.35.−p, 68.37.Ef, 68.49.−h, 68.55.A−

In nanoscience the top down approach uses macroscopic physical properties to influence structure and properties on the nanoscale. The substrate temperature is one of the principal means of controlling the structural phase that is formed. In a situation where there are multiple closely related phases one often finds that these coexist and that we can only vary the relative amounts of material in each phase. To obtain a pure phase in such a case one must look to a means of top down control other than the growth/anneal temperature.

The rare earth silicides are an example of such a binary phase system. They exist in a tetragonal or a hexagonal structural phase when grown on Si(100).[1–12] Two island morphologies are observed; either highly elongated or almost square. The precise morphology obtained depends on the rare earth metal used and the growth temperature but in most cases both island morphologies (and both structural phases) can be seen to coexist on the same surface. Anisotropic lattice matching to the substrate has been suggested as a mechanism to drive the growth of the highly elongated islands with a good lattice match along the growth direction and a large mismatch along the narrow width of the islands. Since the hexagonal unit cell has a larger lattice matching anisotropy than the tetragonal unit cell the elongated islands were assigned to the hexagonal structure and the square islands were believed to be tetragonal. However, the picture is more complex than previously suggested. It was recently found that the elongated holmium silicide islands are in fact tetragonal.[12] Ramírez *et al.*[13] have shown that the diffusion barrier of yttrium is 0.54 eV along the channels between the dimer rows and 1.24 eV across the dimer rows. The implication is that the initial flow of material on the surface is highly anisotropic and mobility as a driving mechanism for the formation of the highly elongated islands must be considered.

One reason for the interest in rare earth silicides on silicon is that the Schottky barrier height (SBH) is low[14–16] which makes thin rare earth layers ideal candidates as buffer layers in, for example, spintronics.[17,18] It has long been known that in nickel silicide the SBH depends on the structural phase and there is a SBH difference of 0.14 eV between a-NiSi and b-NiSi.[19] To control the SBH we first need to control the structural phase. Having achieved this control one might be able to fine tune the barrier height by use of a specific rare earth metal.

At low coverage rare earth silicide nanowires form.[20] These are a few tens of angstrom in width and can grow up to a micron in length and anisotropic lattice matching is again the suggested driving force for growth. To further complicate matters, other low coverage low density periodic arrays of rare earth metals have also been observed between the nanowires.[21–23] It is not yet clear whether these are a precursor to nanowire growth or if this reconstruction exists between the islands at higher coverage.

The system thus presents two different structural phases (tetragonal and hexagonal), two different island morphologies (square and elongated), and two different mechanisms for anisotropic growth (lattice matching and mobility). To exploit the specific properties of each structural phase some means of top down control must be exerted other than the annealing temperature. In this work we have used the mobility of the material during deposition as a control variable to

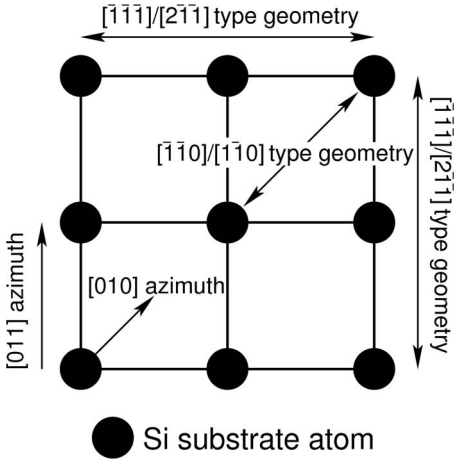

FIG. 1. Top view of the bulk terminated Si(100) surface showing the two incident beam directions used in the MEIS experiments. For the ⟨110⟩ geometry the polar angle with respect to the sample normal was 45° and for the ⟨111⟩ geometry the polar angle was 54.74°.

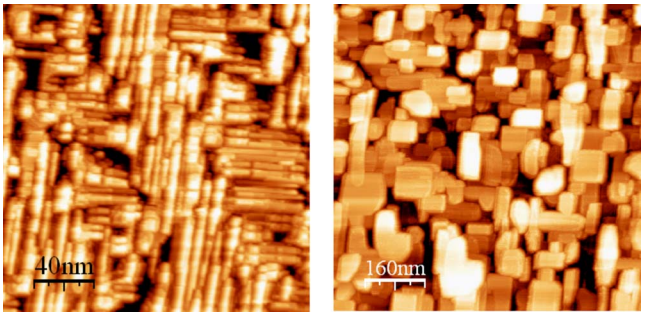

FIG. 2. (Color online) Scanning tunneling microscope images (2 V/2 nA) of holmium silicide islands grown under conditions of high mobility (left) and low mobility (right).

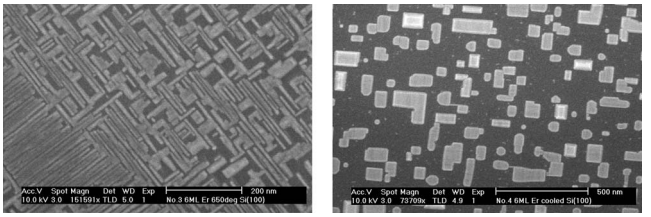

FIG. 3. Scanning electron microscope images of erbium silicide islands grown under conditions of high mobility (left) and low mobility (right) taken after MEIS characterization.

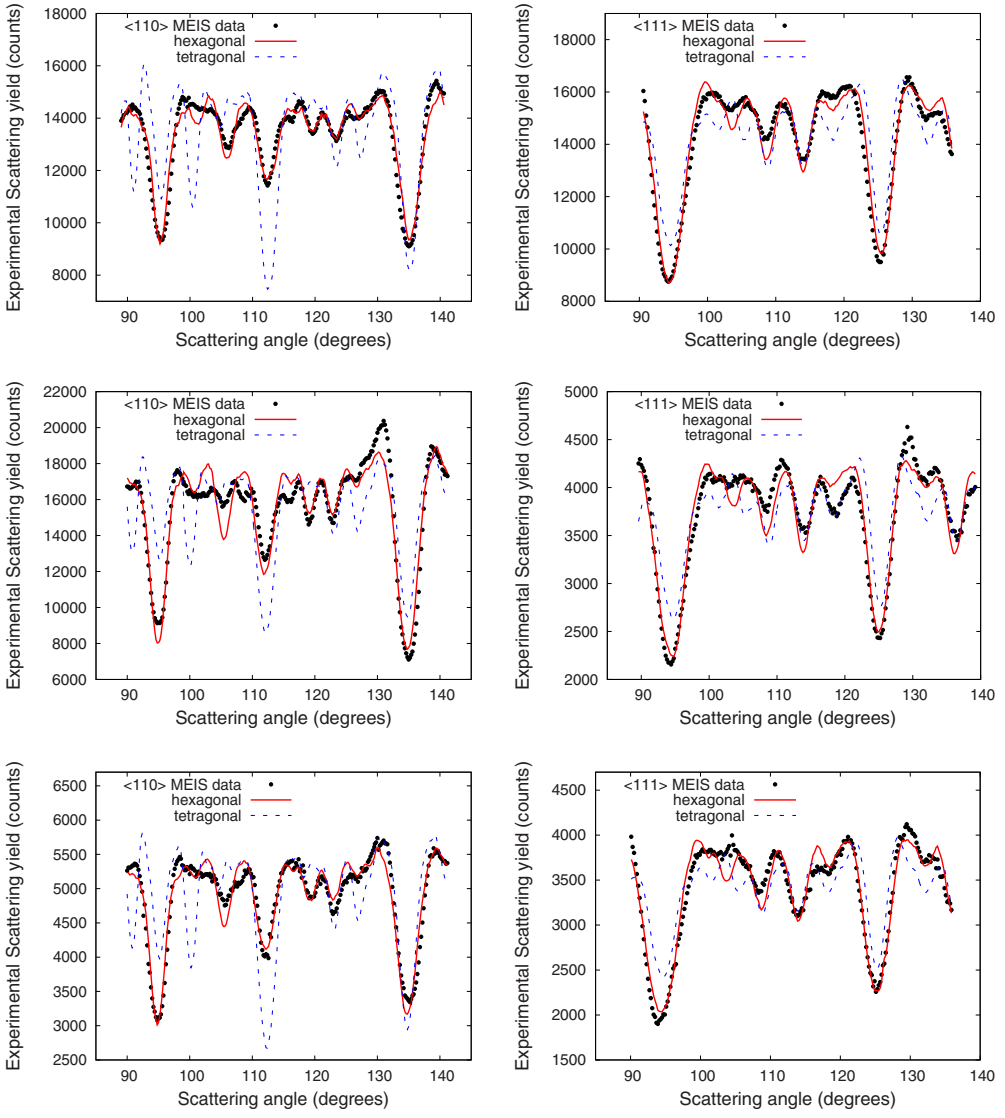

FIG. 4. (Color online) MEIS blocking curves for dysprosium, holmium, and erbium silicide grown on Si(100) by liquid nitrogen cooling the substrate prior to deposition. The left column shows data from the ⟨110⟩ scattering geometry and the right column from the ⟨111⟩ geometry. In each case simulated blocking curves for the known bulk tetragonal and hexagonal phases have been fitted to the data. All three rare earth elements form the hexagonal silicide phase under these growth conditions.

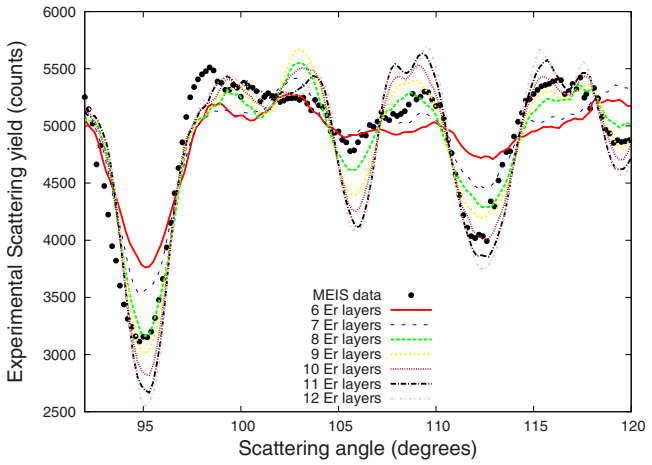

FIG. 5. (Color online) Variation in the thickness of the simulated hexagonal erbium silicide structure model and the effect upon the structure fit. The range of scattering angles has been truncated for clarity. Nine layers produce the best combination of relative blocking dip intensities.

influence the structural phase that results. We find that by suppressing the initial mobility during deposition only the hexagonal phase of dysprosium, holmium, and erbium silicide is formed. Conditions of enhanced mobility during deposition result in the formation of a pure tetragonal phase for holmium silicide and erbium silicide but dysprosium silicide remains as a binary phase.

In the next section we describe how our samples were prepared and analyzed. In Sec. I the effect of mobility on the island morphology is shown using scanning tunneling microscopy (STM) data. The remaining two sections show using medium energy ion scattering (MEIS) data how the island morphology relates to the structure and how control of the initial mobility allows phase selection in the rare earth silicides.

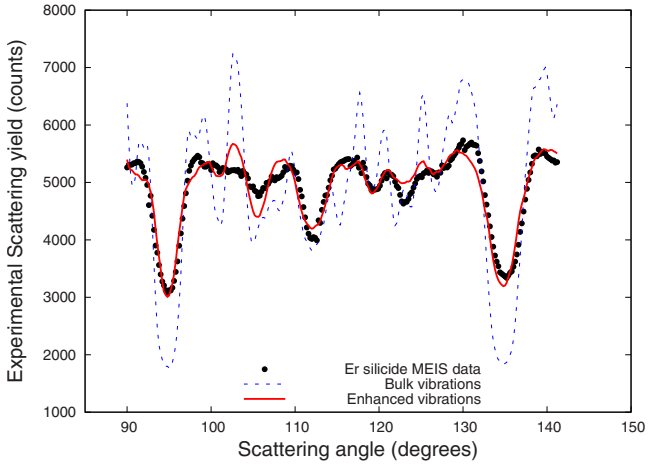

FIG. 6. (Color online) A comparison of MEIS data with simulated blocking curves for hexagonal erbium silicide using the bulk element vibrational amplitudes and amplitudes enhanced by a factor of 2. Enhanced vibrations are crucial in obtaining a good fit to the experimental data indicating that there is static disorder within the islands.

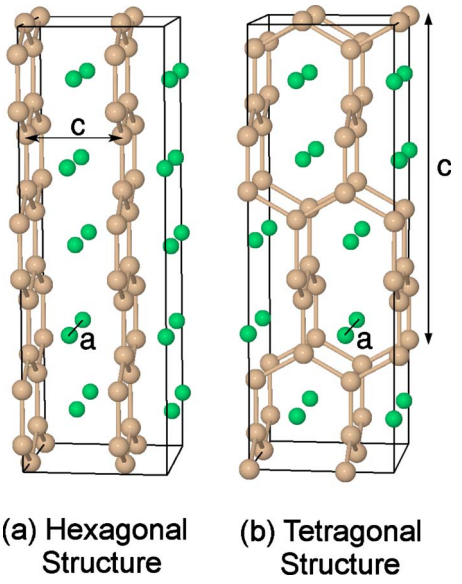

FIG. 7. (Color online) Two structural phases of the bulk rare earth silicides. The bounding box is for perspective and is not the unit cell. In the hexagonal structure the bulk c axis is equal to the spacing of the planes of RE atoms. Silicon atoms are yellow and rare earth atoms are green and shown without bonds. The surface plane is parallel to the a axis in both cases and the cells drawn would sit atop the surface. The interlayer spacings are thus along the vertical direction.

I. SAMPLE PREPARATION AND CHARACTERIZATION

The samples were prepared by depositing 6 ML of the rare earth element onto a clean Si(100) substrate. Si(100) samples were cut from a lightly doped n-type wafer and were outgassed for 15 h at 650 °C. The silicon was cleaned by flash heating to 1200 °C for 30 s, annealing at 900 °C for 10 min followed by a slow cool over about 10 min. The presence of a 2×1 low-energy electron diffraction (LEED) pattern was taken to indicate that the substrate was well ordered after the flash cleaning procedure. Rare earth metal was deposited from an evaporation source of our own design consisting of a rod of metal in a tantalum boat. The sources were calibrated using a quartz crystal microbalance.

Two growth regimes were explored. In the first regime the rare earth was deposited under conditions of low mobility. The Si(100) substrate was precooled to better than 100 K by passing liquid nitrogen through cooling tubes in contact with the end of the manipulator. A thermocouple was used to check the temperature in the vicinity of the sample. 6 ML of material were deposited over 45 min and the substrate cooling was maintained throughout. After deposition the sample was heated to 650 °C and annealed for 45 min. MEIS results for dysprosium, holmium, and erbium silicide samples grown under this regime are presented in Sec. II.

In the second growth regime the rare earth metal was deposited under conditions of high mobility. The substrate was heated to 650 °C prior to deposition and was held at this temperature over the deposition period, which was again 45 min. For both growth methods the same amount of material was deposited and the total deposition time and annealing time was the same. Samples grown in both ways gave a

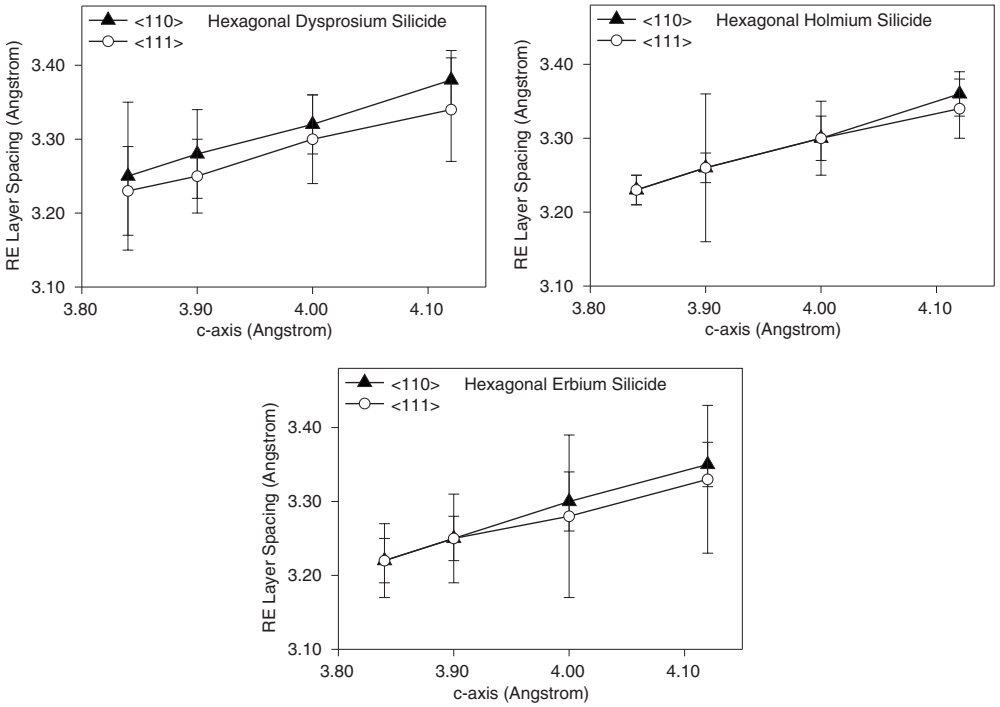

FIG. 8. Fitted interlayer spacings in the hexagonal rare earth silicides for four different epitaxial relationships to the substrate. In each case the *a* axis is fixed at 3.84 Å (that of the silicon substrate) and the interlayer spacings are fitted for different *c*-axis values. In the bulk the respective *c* axes are 4.12, 4.10, and 4.09 Å. These bulk *c* axes give interlayer spacings that do not distort the bond angles in the graphitic silicon layers.

$c(2\times2)$ LEED pattern. MEIS results for dysprosium and erbium silicide samples grown under this regime are presented in Sec. III. In a previous study we presented work for holmium silicide grown in this manner.[12]

For structural characterization we have used MEIS. The principle of this technique is that a beam of protons is directed into the sample along a known cystallographic direction. Atoms in the bulk are shadowed by surface atoms and ions can only be scattered by the surface region of the material. At the beam energy of 100 keV the scattering process can be represented using simple classical Rutherford scattering and the energy of a scattered ion can be used to determine which element in the surface it has interacted with. In the case of the rare earth silicides the large mass separation between silicon and the rare earth allows for complete resolution of the scattered yields off the two elements. Angular projection of the scattered ion yield reveals dips in the scattered intensity along certain angular directions where surface atoms have blocked the scattered ions on the way out of the crystal. The ability of MEIS to resolve the ions scattered off the rare earth atoms in the surface and to fingerprint the structure using the blocking pattern makes it an ideal technique for structural studies of our rare earth silicide samples.

MEIS data were taken at the UK MEIS facility at STFC Daresbury Laboratory. Samples were grown under ultrahigh vacuum (UHV), with typical base pressures of 2×10^{-10} mbar and then transferred under UHV into the scattering chamber. The ion beam was 100 keV H^+ ions and the scattered ions were detected using an angle-resolving toroidal-sector electrostatic ion-energy analyzer and a microchannel plate detector. The MEIS spectra confirmed that the samples were free of contaminants and data were acquired with a total dose of $\sim10^{16}$ ions cm^{-2}. Further details about the Daresbury MEIS facility can be found in the literature.[24–28] During each experiment two different incident beam directions were used and these are shown with respect to the substrate in Fig. 1. The notation $[in]/[out]$ for each geometry defines the ingoing crystal direction $[in]$ and an outgoing crystal direction $[out]$ that lies in the detected angular range of the scattered ions. To interpret the blocking pattern it is compared to one that has been simulated using Monte Carlo methods contained in the XVEGAS code.[29] A proposed model structure can be fitted to the experimental data by independent variation in the atomic positions and the

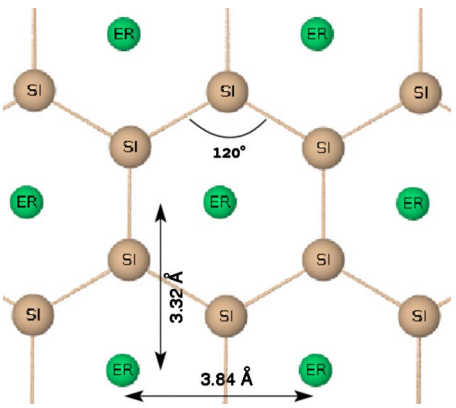

FIG. 9. (Color online) Hexagonal erbium silicide viewed along the **c** axis. With an epitaxial **a** axis an interlayer spacing of 3.84 Å $\times\cos 30° = 3.32$ Å will maintain the hexagonal symmetry and the bond angles within the graphitic silicon layers.

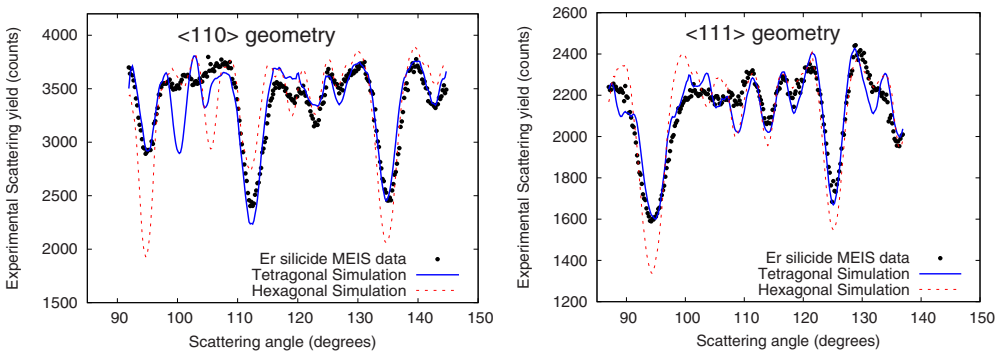

FIG. 10. (Color online) MEIS blocking curves for erbium silicide grown under conditions of high mobility taken in the ⟨110⟩ and the ⟨111⟩ scattering geometries. XVEGAS simulated blocking curves for the known bulk tetragonal and hexagonal phases have been fitted to the data and these clearly identify the tetragonal structure.

atomic vibrations and the quality of the fit is measured using a MEIS R-factor.

Before the more extensive structural studies using MEIS were undertaken an illustrative growth study was done using an Omicron Nanotechnology GmbH STM with a typical base pressure of 2×10^{10} mbar to characterize the island morphologies and optimize the growth conditions. These results are outlined in the next section.

II. STM STUDY OF THE ISLAND MORPHOLOGIES

Figure 2 shows images taken with a scanning tunneling microscope of holmium silicide samples prepared by depositing the holmium under conditions of high mobility and with the substrate cooled with liquid nitrogen to reduce the mobility. High initial mobility causes densely packed elongated islands to form and reduced initial mobility results in much larger islands that are closer to being square in shape.

The samples for MEIS analysis were grown *in situ* and we used electron beam heating to anneal our samples. In the STM experiments we used direct current heating. To ensure that the island morphology was consistent between the different UHV growth systems with their different heating methods we have imaged our MEIS samples in an electron microscope a few days after removal from the UHV environment. Figure 3 shows electron microscope images of erbium silicide islands grown in the MEIS chamber. The two growth regimes produce a similar morphology to that seen in the STM experiments. We have analyzed samples with these different morphologies using MEIS and the results are presented in the next two sections.

III. GROWTH ON A LIQUID NITROGEN COOLED SUBSTRATE

Figure 4 shows MEIS blocking curves for dysprosium, holmium, and erbium silicide islands grown by deposition onto a liquid nitrogen cooled substrate. The data for both beam geometries have been fitted to the hexagonal and tetragonal silicide structures using the XVEGAS code. For each system in both geometries the MEIS blocking pattern can be unambiguously identified as the hexagonal silicide phase.

In the rest of this section we will outline how the hexagonal structure was fitted to the data and what this process has revealed about the structure, epitaxy, and the disorder within the hexagonal silicides. The thickness of the silicide has a significant effect upon the relative intensity of the blocking curves (but not the angular positions of the major features) and if the simulated structure is too thick then extra blocking dips can occur that are not present in the data. Figure 5 shows how the fit to the ⟨110⟩ erbium silicide MEIS data is affected by variation in the number of erbium layers (each erbium layer carries with it two associated silicon layers). To reproduce the relative dip intensities in the MEIS data at least eight layers must be included in the simulation. More than ten layers causes the blocking dips to become too deep and also introduces extra dips that are not present in the MEIS data (see the dips at scattering angles of 108° and 117°, for example). The best fit is an average of the island heights over the surface and means the dysprosium, holmium, and erbium silicide islands were around 30 Å thick with a small variation across the series.

Having optimized the number of layers to include in the simulation the full model structure was fitted to the MEIS data. The roughness of the sample is not a significant factor when fitting the atomic positions as these are most sensitive to the angular positions of the blocking dips. At first the crystals were stretched along the vertical direction until the blocking dips were approximately fitted. Then the XVEGAS program was used to optimize the position and the vibrations of each atom along each degree of freedom. A multidimensional search algorithm was used to efficiently drive the fit toward a minimum with respect to all degrees of freedom. It was found that the optimum vibrational amplitudes of all of the atoms in x, y, and z were twice the value in the bulk for all three systems in both geometries. We believe that such a large vibrational amplitude reflects static disorder in the atomic positions and not dynamic disorder. Other workers have seen evidence for this using transmission electron microscopy (TEM).[8,11] The static disorder in our MEIS results could also contain a significant contribution from the "roughness" of different island heights. Figure 6 shows the effect of restoring the vibrations back to their bulk values. The simulated blocking dip intensities become very poor and extra blocking dips are introduced along with splitting of existing blocking dips.

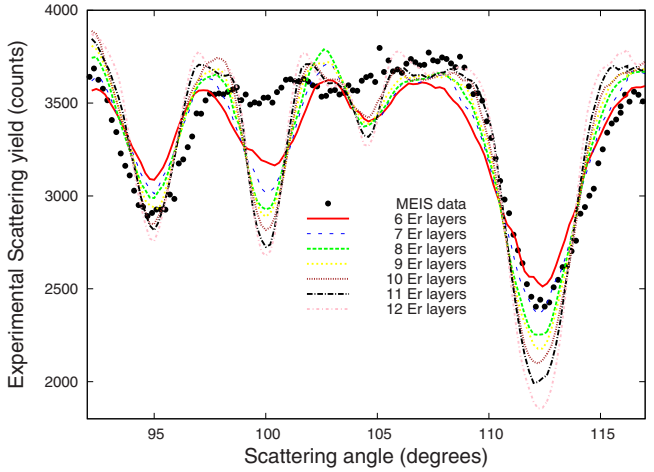

FIG. 11. (Color online) Variation in the thickness of the simulated tetragonal erbium silicide structure model and the effect upon the structure fit for the ⟨110⟩ direction. The range of scattering angles has been truncated for clarity. Eight layers produce the best combination of relative blocking dip intensities.

With the correct number of layers and with enhanced vibrations to account for static disorder the interlayer spacings can now be fitted. However, one more factor must be taken into consideration and that is the epitaxial relationship of the islands with the substrate. In MEIS it is not possible to uniquely obtain the lateral lattice parameters of fitted crystals. If the lateral spacings in the crystal are increased then the angular position of a blocking dip can be maintained by an increase in the vertical spacings.

In the surface plane there are the **a** and **c** lattice spacings (see Fig. 7). TEM results[11] show that the **a** axis is epitaxial and the **c** axis is incommensurate. In our MEIS simulations we have set the value of the **a** axis at the silicon lattice spacing (3.84 Å). Since we cannot determine the **c** axis uniquely we have structure fitted the interlayer spacings for

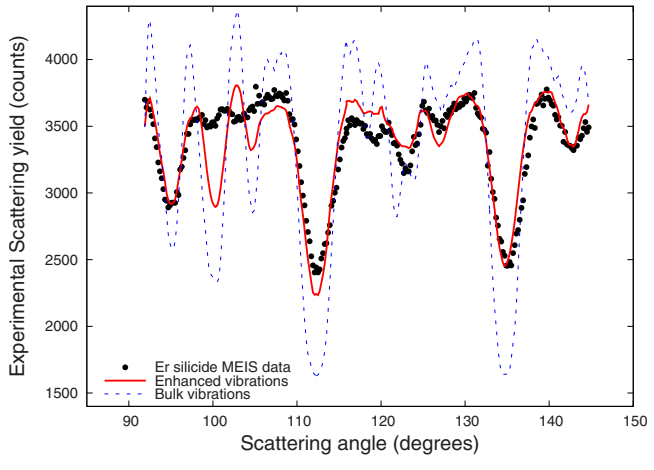

FIG. 12. (Color online) A comparison of MEIS data with simulated blocking curves for tetragonal erbium silicide using the bulk element vibrational amplitudes and amplitudes enhanced by a factor of 2. Enhanced vibrations are crucial in obtaining a good fit to the experimental data indicating that there is static disorder within the islands.

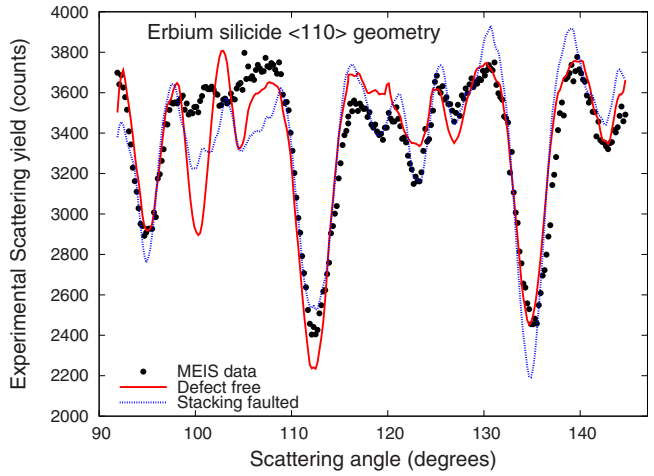

FIG. 13. (Color online) Simulation of tetragonal erbium silicide with a stacking fault. A better fit with the MEIS data is seen in the region 115°–130° and the weak dips in the MEIS data at 99° and 102° are better accounted for.

several *c* axes starting with an epitaxial fit and moving to the bulk spacing. Figure 8 shows our fitted structural parameters for hexagonal dysprosium, holmium, and erbium silicide. The error bars are derived from the linear regression fit as the interlayer spacings pass through the best-fit value as they are stretched and compressed. Holmium and erbium silicide have very similar interlayer spacings which is to be expected since the bulk crystals are almost identical in size. Dysprosium silicide has a larger **c** axis and the layer spacings are slightly higher.

Figure 9 shows the hexagonal crystal viewed along the **c** axis. With perfect hexagonal symmetry the interlayer spacing is 3.32 Å and in Fig. 8 we can see that this would correspond to an incommensurate **c** axis in all three cases. The **c** axis is thus closely related to the hexagonal symmetry of the crystal.

IV. GROWTH UNDER CONDITIONS OF HIGH MOBILITY

A. Erbium silicide

Figure 10 shows the best fit obtained for the hexagonal and tetragonal structures to the MEIS data from erbium silicide grown under conditions of high mobility. The relative intensities of the blocking dips reveal that this structure is tetragonal. We have intermixed the simulated hexagonal and tetragonal blocking curves in various ratios but no improvement is seen in the R-factor when any amount of hexagonal silicide is included. Thus we must conclude that under conditions of high mobility erbium silicide forms elongated islands that have a tetragonal structure.

Having identified this pure phase we can now begin to gather further details from the blocking curves, the first of which is the thickness of the silicide. Figure 11 shows simulated blocking curves for various thicknesses of erbium silicide. We can see that eight layers ensures that the relative intensities are optimal which corresponds to average silicide thickness of around 25 Å.

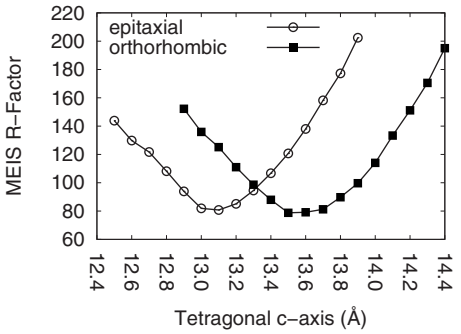

FIG. 14. Fitting of the **c** axis of tetragonal erbium silicide. As the crystal is laterally compressed to become epitaxial the **c** axis becomes smaller, presumably to prevent distortion of the bond angles.

The region of the simulations with a scattering angle in the range 98°–106° is a poor fit to the MEIS data in both the ⟨110⟩ and ⟨111⟩ geometries. We might expect that static disorder might be responsible for weakening the dip intensities just as we saw in the last section for the hexagonal silicides. Indeed a full fit of each spatial and vibrational degree of freedom again suggests enhanced vibrations (see Fig. 12). However, these are not sufficient to account for the weakened intensities. There remain two other possibilities. The first is the surface termination but we have found that the MEIS blocking dips are relatively insensitive to a change in position of the surface silicon atoms.

The second possibility is suggested by TEM. Images in the literature[8,11] show that stacking faults are often present in the tetragonal islands. Figure 13 shows a simulation where a stacking fault has been introduced half way up the tetragonal island. Significant improvement is seen in the fit for the 116°–129° region of scattering angles. The intensity of the blocking dip at 99° is also reduced favorably toward that of the experimental dip. The relative intensity of the three principal dips (95°, 112°, and 135°) is affected but it is expected that this can be repaired by adjusting the number of layers included. There are good indications that the effect of stacking faults is present in the MEIS data but to fully account for this one would have to simulate many large islands with randomly located stacking faults and then perform an average.

No tetragonal phase of erbium silicide has yet been identified in the bulk or in thin film form. To understand the epitaxy we have used the orthorhombic lattice constants of bulk $HoSi_2$ (**a**=4.03 Å, **b**=3.94 Å, and **c**=13.30 Å) since these adjacent elements have similar lattice constants in the hexagonal silicide phase. Note that the **c** axis for the tetragonal silicides is defined as being perpendicular to the surface and not parallel to it as in the case of the hexagonal silicides. Figure 14 shows the minimum in the MEIS R-factor as the **c** axis is varied in the case of an epitaxial and an orthorhombic

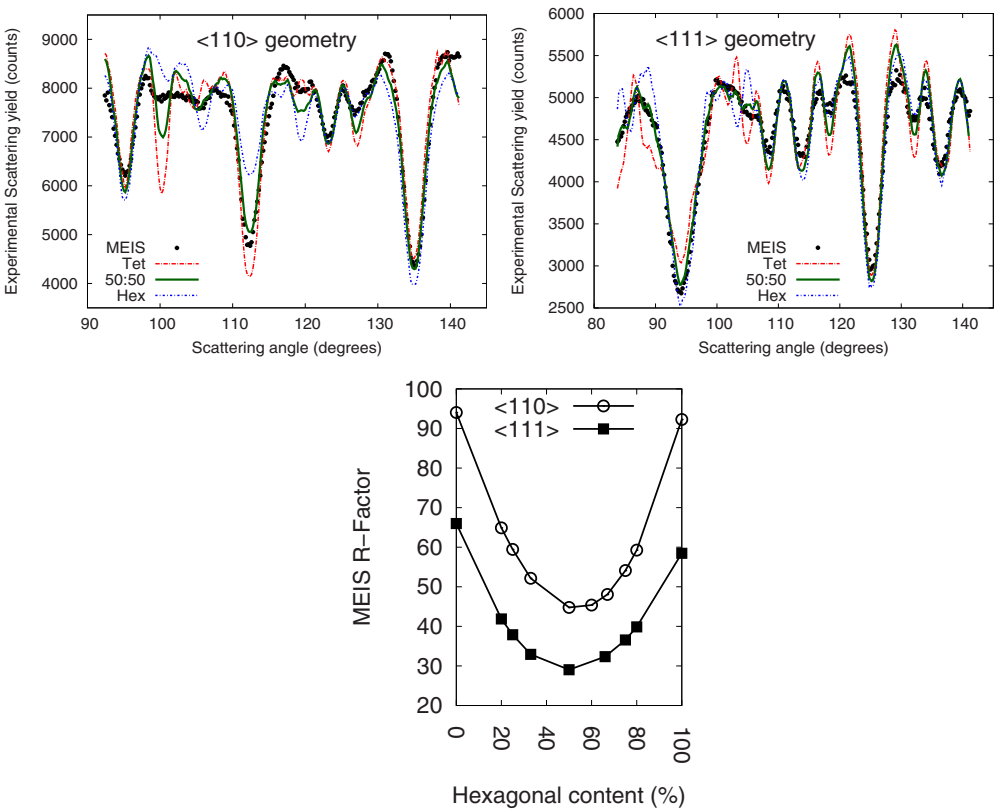

FIG. 15. (Color online) For dysprosium silicide grown under high mobility conditions a comparison of experimental MEIS blocking curves with best-fit XVEGAS simulated blocking curves for the tetragonal and hexagonal phases of dysprosium silicide in the ⟨110⟩ and the ⟨111⟩ scattering geometries. Summed curves representing different relative amounts of hexagonal and tetragonal islands have also been compared. The MEIS R-factor is shown against this ratio in the bottom figure and it suggests that the two phases exist in an equal ratio.

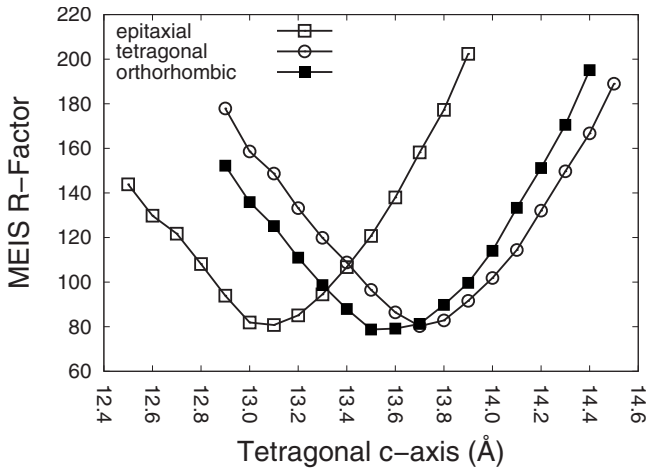

FIG. 16. Optimization of the tetragonal *c* axis for crystals with three different lateral dimensions. For an epitaxial crystal (**a**=**b** =3.84 Å) the *c* axis is 13.1 Å. A tetragonal crystal (**a**=**b** =4.03 Å) gives a *c* axis of just under 13.6 Å and an orthorhombic crystal (**a**=4.04 Å, **b**=3.92 Å) gives **c**=13.8 Å. There is thus a positive correlation between the lateral lattice constants and the vertical spacings.

crystal. The lateral lattice constants are proportional to the vertical lattice constants as in the hexagonal silicides and we suspect that a similar process is occurring whereby the bond angles are maintained.

B. Dysprosium silicide

Figure 15 shows MEIS blocking curves for dysprosium silicide islands grown under conditions of high mobility. Tetragonal and hexagonal blocking curves have been fitted to the data but neither structure is favored in isolation. The simulated blocking patterns have been intermixed and the MEIS R-factor suggests that an approximate 50:50 mixture of the two structures is present.

Again, enhanced vibrations were required to match the blocking dip intensities and we also see evidence for stacking faults as in the case of erbium silicide (see Fig. 13). The experimental data are thus a convolution of scattered yields from hexagonal and tetragonal islands that contain significant amounts of short-range disorder and stacking faults. Further fitting of the data is thus not possible because there are not precise atomic positions to fit.

The epitaxial relationship with the substrate is shown in Fig. 16. The variation in the MEIS R-factor around the optimum value is shown as the **c** axis is stretched and compressed. In the same manner as we showed for the hexagonal silicides and tetragonal erbium silicide a lateral compression of the crystal results in a contraction of the **c** axis.

V. DISCUSSION

In summary we have shown that when dysprosium, holmium, and erbium are deposited onto a liquid nitrogen cooled substrate the hexagonal structural phase is formed after annealing. When erbium is deposited onto a hot substrate only the tetragonal phase results. For dysprosium silicide growth under conditions of high mobility causes approximately equal numbers of hexagonal and tetragonal islands to form. Mobility during growth is of such importance in the rare earth silicides that it can dictate which structural phase is formed.

A key question is raised; why do the tetragonal islands show strong anisotropy in their growth direction when it is the hexagonal silicides that have the greater lattice anisotropy? Our work seems to suggest that lattice anisotropy is not as strong a driving mechanism for causing elongated island growth or nanowire growth as was previously believed. We have repeated these experiments at low coverages (0.6 ML) and we find that it is not possible to grow nanowires after deposition onto a liquid nitrogen cooled substrate. This would suggest that the growth mechanism of nanowires requires that the rare earth atoms be mobile on a clean surface so they can flow and form a wire. This could be related to the presence of the silicon dimers on the clean surface. It has been shown that anisotropic mobility depends on the presence of the dimer rows. Where the dimer rows remain intact a natural channel is formed along which rare earth atoms can flow with high mobility to interconnect and form a nanowire. If the surface has a high coverage of rare earth atoms before annealing is started then when thermal energy is made available nucleation into square islands occurs. The internanowire reconstruction that occurs could prevent nanowire formation rather than be a precursor for it. One piece of evidence to support this is the fact that on a vicinal surface extremely long (1 μm) nanowires can be formed using very low coverage but if the coverage is too high nanowire growth is stunted. The implication that the elongated islands are tetragonal also throws some doubt upon the idea that nanowires are hexagonal in structure as does recent theoretical work showing that on the clean surface tetragonal nanowires are lower in energy than hexagonal nanowires.[30] When considering the epitaxy of the islands with the substrate a constant theme in all of the fitting procedures has been that the vertical spacings in the crystal are proportional to the lateral dimensions of the crystal. Intuitively one might expect the opposite to be true; that compression of the crystal in one dimension might result in expansion in the other in order to maintain the volume in accordance with the theory of Poisson ratios. However, this theory is a macroscopic effect and within our nanoscale materials quantum mechanics seems to dictate the behavior by preventing distortion of the bond angles.

It would be interesting to see the results of density-functional theory calculations to see which phase is more stable (with a Gibbs free-energy correction to account for the different number of atoms in the unit cell). It is also possible to look at the lateral bulk modulus to see which phase is more compressible.

Finally, it would be very interesting now to look for differences in the properties of these phase selected islands. For example, we would like to know if there is a Schottky barrier height difference between the two phases for a given rare earth element and also if there is a trend in this barrier height along the series of rare earths for a given structural phase.

*spt1@york.ac.uk

[1] C. Preinesberger, S. Vandré, T. Kalka, and M. Dähne-Prietsch, J. Phys. D: Appl. Phys. **31**, L43 (1998).
[2] N. Frangis, G. Van Tendeloo, J. Van Landuyt, G. Kaltsas, A. Travlos, and A. G. Nassiopoulos, Phys. Status Solidi A **158**, 107 (1996).
[3] N. Frangis, J. V. Landuyt, G. Kaltsas, A. Travlos, and A. G. Nassiopoulos, J. Cryst. Growth **172**, 175 (1997).
[4] G. Chen, J. Wan, J. Yang, X. Ding, L. Ye, and X. Wang, Surf. Sci. **513**, 203 (2002).
[5] B. Z. Liu and J. Nogami, J. Appl. Phys. **93**, 593 (2003).
[6] B. Z. Liu and J. Nogami, Nanotechnology **14**, 873 (2003).
[7] Q. Cai and W. Zhou, J. Phys.: Condens. Matter **16**, 6835 (2004).
[8] Z. He, D. J. Smith, and P. A. Bennett, Phys. Rev. B **70**, 241402(R) (2004).
[9] G. Ye, J. Nogami, and M. A. Crimp, Thin Solid Films **497**, 48 (2006).
[10] G. Ye, M. A. Crimp, and J. Nogami, *Self-Assembled GdSi2 Nanostructures Grown on Si(001)*, MRS Symposia Proceedings No. 901 (Materials Research Society, Pittsburgh, 2006), p. Ra13.
[11] J. Zhang, M. A. Crimp, Y. Cui, and J. Nogami, J. Appl. Phys. **103**, 064308 (2008).
[12] T. J. Wood, C. Eames, C. Bonet, M. B. Reakes, T. C. Q. Noakes, P. Bailey, and S. P. Tear, Phys. Rev. B **78**, 035423 (2008).
[13] A. Ramírez, G. H. Cocoletzi, G. Canto, and N. Takeuchi, Surf. Sci. **603**, 3414 (2009).
[14] K. N. Tu, R. D. Thompson, and B. Y. Tsaur, Appl. Phys. Lett. **38**, 626 (1981).
[15] S. Vandre, T. Kalka, C. Preinesberger, I. Manke, H. Eisele, M. Dahne-Prietsch, R. Meier, E. Weschke, and G. Kaindl, Appl. Surf. Sci. **123-124**, 100 (1998).
[16] H. Norde, J. de Sousa Pires, F. d'Heurle, F. Pesavento, S. Petersson, and P. A. Tove, Appl. Phys. Lett. **38**, 865 (1981).
[17] M. B. Reakes, C. Eames, and S. P. Tear, J. Phys.: Condens. Matter **21**, 265001 (2009).
[18] Z. Z. L. Geng, B. Magyari-Kope, and Y. Nishi, IEEE Electron Device Lett. **29**, 746 (2008).
[19] R. T. Tung, Phys. Rev. Lett. **52**, 461 (1984).
[20] J. H. G. Owen, K. Miki, and D. R. Bowler, J. Mater. Sci. **41**, 4568 (2006).
[21] C. Ohbuchi and J. Nogami, Phys. Rev. B **66**, 165323 (2002).
[22] A. Pratt, C. Woffinden, C. Bonet, and S. Tear, Phys. Rev. B **78**, 155430 (2008).
[23] M. P. J. Punkkinen, M. Kuzmin, P. Laukkanen, R. E. Perälä, M. Ahola-Tuomi, J. Lång, M. Ropo, M. Pessa, I. J. Väyrynen, K. Kokko, B. Johansson, and L. Vitos, Phys. Rev. B **80**, 235307 (2009).
[24] D. J. Spence, S. P. Tear, T. C. Q. Noakes, and P. Bailey, Phys. Rev. B **61**, 5707 (2000).
[25] D. J. Spence, T. C. Q. Noakes, P. Bailey, and S. P. Tear, Surf. Sci. **512**, 61 (2002).
[26] D. J. Spence, T. C. Q. Noakes, P. Bailey, and S. P. Tear, Phys. Rev. B **62**, 5016 (2000).
[27] C. Bonet, I. M. Scott, D. J. Spence, T. J. Wood, T. C. Q. Noakes, P. Bailey, and S. P. Tear, Phys. Rev. B **72**, 165407 (2005).
[28] T. J. Wood, C. Bonet, T. C. Q. Noakes, P. Bailey, and S. P. Tear, Surf. Sci. **598**, 120 (2005).
[29] J. W. M. Frenken, J. F. van der Veen, and R. M. Tromp, Nucl. Instrum. Methods Phys. Res. B **17**, 334 (1986).
[30] C. Eames, M. I. J. Probert, and S. P. Tear, Appl. Phys. Lett. **96**, 241903 (2010).